Chemical Science

ROYAL SOCIETY OF CHEMISTRY

EDGE ARTICLE

View Article Online
View Journal | View Issue

Cite this: *Chem. Sci.*, 2025, **16**, 15355

All publication charges for this article have been paid for by the Royal Society of Chemistry

Received 30th May 2025
Accepted 5th July 2025

DOI: 10.1039/d5sc03778f

rsc.li/chemical-science

Novel tryptophan 2,3-dioxygenase-targeted ruthenium(II)-indole complex activates immunotherapy *in vitro* and *in vivo*†

Zheng-Qi Shen,‡ Binglian Guo,‡ Xiangyu Dai,‡ Hanxue Liu, Meng Ren, Peisen Wang, Yating Zhang, Yinuo Xu, Zhi Su, Xuling Xue* and Hong-Ke Liu *

Immunotherapy targeting immune checkpoints has emerged as a promising strategy in cancer treatment; however, the heterogeneous and dynamic tumor microenvironment (TME) imposes critical constraints on therapeutic outcomes. Tryptophan 2,3-dioxygenase (TDO), often dysregulated in malignant tissues, plays a pivotal role in shaping an immunosuppressive milieu by depleting tryptophan, thereby hindering anti-tumor immune response. To counteract this immune evasion mechanism, we designed a novel indole-coordinated ruthenium(II) arene complex (**In-Ru**), aimed at bolstering tumor immunotherapy and thwarting immune evasion by targeting TDO expression. Our findings reveal that **In-Ru** exerts markedly potent anti-proliferative effects against HepG2 cells. It achieves this by specifically localizing to the cell nucleus, inducing DNA damage, and initiating a cascade of necroptosis as well as immunogenic cell death (ICD), thereby potentially enhancing the immune system's capacity to recognize and attack cancer cells. RNA sequencing and qRT-PCR analysis indicate that **In-Ru** modulates pathways linked to tryptophan metabolism and immune reprogramming, with specific degradation of TDO protein and reversal of tryptophan-mediated immunosuppression. Furthermore, TDO inhibition boosts ROS production and induces necroptosis *via* mitochondrial damage, triggering a strong immune response. The tumor vaccine experiment revealed that **In-Ru** significantly reduced TDO levels and triggered ICD effect in liver cancer animal models. By reversing the immunosuppressive microenvironment, **In-Ru** facilitated the maturation of dendritic cells (DCs) and promoted T-cell infiltration, thereby achieving robust anti-tumor efficacy and long-lasting immune protection. This study represents the first report of a metal-arene complex with dual functions of TDO inhibition and ICD induction. It not only enhances anti-tumor immunogenicity but also effectively mitigates the risk of immune overactivation, offering a precise regulatory paradigm for the development of metal-based complexes in tumor immunotherapy.

Introduction

Platinum complexes have achieved remarkable breakthroughs in biomedical research.[1,2] Motivated by these advances, significant efforts have been devoted to exploring the biological mechanisms of other metal complexes.[3–11] In recent years, extensive studies have demonstrated that metal-arene complexes (*e.g.*, ruthenium, iridium, and rhodium) exhibit innovative anti-tumor mechanisms and enhanced safety profiles compared to traditional platinum drugs.[12] These properties enable them to markedly reduce systemic toxicity and circumvent chemotherapy resistance. Then, metal-arene complexes possess superior lipid solubility and cell membrane permeability. Through structural optimization, they can facilitate extensive intracellular accumulation and precise subcellular organelle targeting.[13] Building on our prior research,[3,14–22] we introduced a metal–ligand synergistic enhancement (MLSE) strategy, which uses the cooperative effects of metal precursors and organic ligands to design and synthesize Ru/Ir complexes for tumor immunotherapy. Among these, **Ir-Bet** can evoke ferroptosis for synergistic enhancement of immunotherapy,[14] whereas **RuBTB** can trigger immunogenic ferroptosis for reverse drug resistance.[19] Furthermore, we successfully achieved the *in situ* synthesis of Ru(II) arene complex (**Ru-rhein**) within tumors, enabling the precise fabrication of metal anti-tumor complex and proposing a "bio-orthogonally catalyzed lethality" strategy.[17] These findings highlight the therapeutic potential and unique advantages of metal-arene complexes in tumor immunotherapy, as well as their applicability for *in situ* drug synthesis.

Jiangsu Collaborative Innovation Center of Biomedical Functional Materials, School of Chemistry and Materials Science, Nanjing Normal University, Nanjing 210023, China. E-mail: xuexuling87@163.com; liuhongke@njnu.edu.cn

† Electronic supplementary information (ESI) available. See DOI: https://doi.org/10.1039/d5sc03778f

‡ Zheng-Qi Shen, Binglian Guo and Xiangyu Dai contributed equally to this work.

Hepatocellular carcinoma (HCC) is one of the most prevalent malignant tumors, marked by high incidence and mortality rates.[23] Moreover, patients with HCC often exhibit a poor prognosis due to the propensity for secondary metastasis to occur in multiple organs, which ultimately contributes to treatment failure and death.[24] Tryptophan 2,3-dioxygenase (TDO) serves as a rate-limiting enzyme in the conversion of L-tryptophan to L-kynurenine.[25] It is aberrantly overexpressed in various cancers, particularly in HCC tissues, where its levels are significantly elevated compared to those in normal liver tissues.[26] Clinical studies have demonstrated that TDO directly drives the progression of HCC by regulating metabolism, inducing the differentiation of regulatory T cells (Tregs), and suppressing the activity of effector T cells, thereby mediating tumor immune escape.[27] Recent reports highlight that TDO represents a promising therapeutic target for HCC treatment. Reducing TDO levels in cancer cells not only alleviates tryptophan depletion but also potentiates anti-tumor immune response.[28,29] Consequently, the development of novel TDO inhibitors for HCC therapy could effectively mitigate immune resistance during treatment, offering new opportunities for clinical intervention.

TDO serves as a prototypical immunosuppressive checkpoint that facilitates tumor immune evasion.[30] It catalyzes the catabolism of tryptophan *via* the KYN pathway, leading to tryptophan depletion and the accumulation of downstream metabolites aryl hydrocarbon receptor (AhR).[25,31] This metabolic shift promotes the differentiation of immunosuppressive DCs and Tregs, which collectively establish an immunosuppressive microenvironment that accelerates tumor immune escape. Dolusic pointed for the first time that indole compounds exhibit structural similarities to tryptophan, enabling them to act as inhibitors of TDO.[32] This action reduces tryptophan catabolism and elevates local tryptophan concentrations, thereby enhancing the efficacy of immunotherapy. Although TDO and IDO are key enzymes in the tryptophan metabolic pathway and contribute to tumor immune escape,[30] studies on metal complexes targeting TDO are relatively scarce, particularly metal-arene complexes, which have not yet been reported. Very few metal-based complexes incorporating indole ligands have been reported to function as TDO inhibitors. Gou reported a platinum(IV) complex coordinated by an indole ligand,[33,34] which suppresses TDO expression, modulates T cell activation and proliferation only *in vivo*. It remains challenging to elucidate the correlation between TDO inhibition and immune activation by metal complexes in HCC animal models due to insufficient evaluation of immune effects at the *in vitro* level, and the lack of systematic investigations into their impacts on the TDO-related immune microenvironment.

To address the above challenges of TDO inhibition and immune activation by metal complexes in HCC therapy, this work innovatively designed and synthesized a novel indole-coordinated Ru(II) arene complex (**In-Ru**). By using the MLSE strategy, this complex aims to simultaneously exert chemotherapeutic effects and inhibit TDO expression, thereby enhancing the immunotherapeutic efficacy. The experiment results demonstrate that **In-Ru** accumulates significantly in the cell nucleus, by inhibiting the TDO pathway, potentiates necroptosis induced by ROS accumulation and mitochondrial membrane potential collapse. Necroptosis triggers cell membrane rupture and the release of damage-associated molecular patterns (DAMPs), thereby inducing ICD effect and subsequently activating systemic anti-tumor immune responses. RNA sequencing and qRT-PCR analysis demonstrated that **In-Ru** significantly suppresses TDO expression in HepG2 cells, concomitant with the inactivation of the AhR signaling pathway, thereby effectively inhibiting tryptophan metabolism-mediated immune escape. *In vivo* vaccine experiments revealed that **In-Ru** specifically attenuates TDO activity within mouse tumors, thereby enhancing anti-tumor immunity. Furthermore, the complex induces ICD effect, promoting DCs maturation and T-cell activation, which in turn triggers systemic immune protection and tumor ablation. As the first metal complex-based ICD inducer targeting the TDO pathway, this study systematically elucidated the molecular mechanism by which metal-arene complexes mediate the integration of chemotherapy and immunotherapy *via* the TDO-AhR axis. A novel "chemotherapy sensitization-immunoregulation" tumor treatment paradigm was successfully established, offering new perspectives for the immunotherapy of solid tumors (Fig. 1).

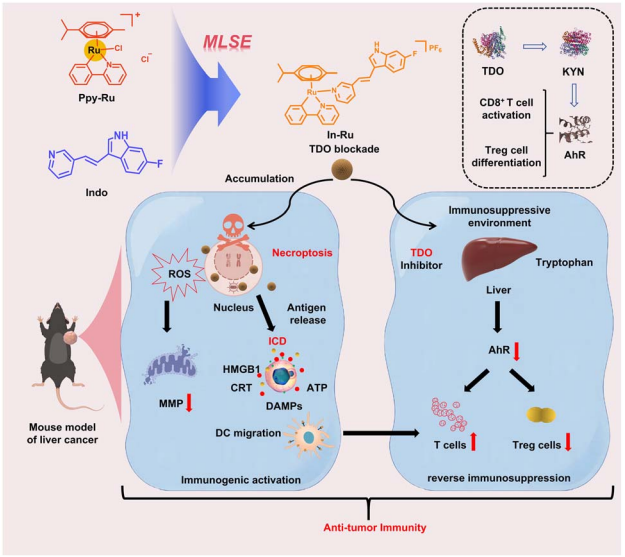

Fig. 1 By using the metal–ligand synergistic enhancement (MLSE) strategy, a novel TDO metal-based TDO inhibitor **In-Ru** was successfully developed. **In-Ru** reverses the immunosuppressive microenvironment through the inhibition of the TDO-KYN-AhR pathway, at the same time can induce cell necroptosis and enhances the efficacy of immunogenic cell death, and consequently activates relevant immune cells to augment the anti-tumor immune response.

Results and discussion

Synthesis and characterization

Metal complexes **In-Ru** and **In-Ir** were synthesized following previously reported procedures.[14] The functional ligand Indo and metal precursors (Ppy-Ru, Ppy-Ir) were synthesized with

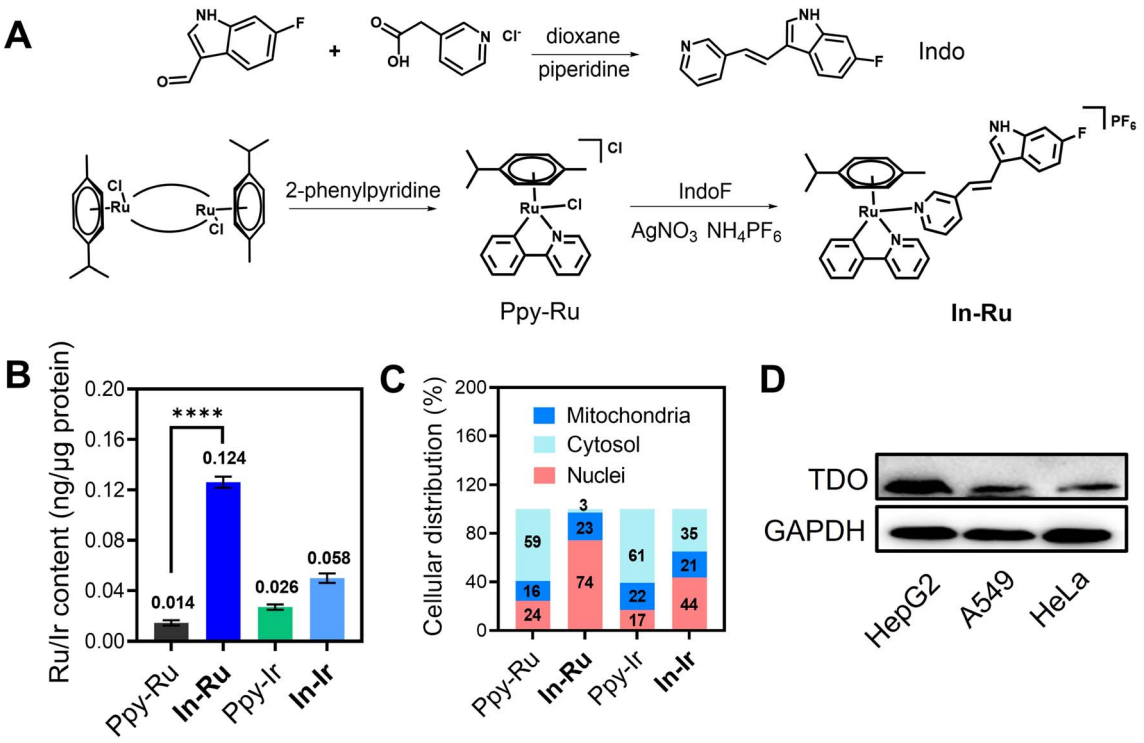

E

Compound	IC_{50} values toward different cell lines for 48 h (μM)			
	HepG2	A549	HeLa	HLF
Indo	77.3±0.9	85.9± 0.6	86.8±0.8	102.4±1.1
Ppy-Ru	73.1±0.7	76.4±0.3	74.1±1.1	89.2±0.5
In-Ru	**3.6±0.2**	**6.9 ±0.5**	**6.8±0.1**	**11.4±0.1**
Ppy-Ir	28.5±0.9	27.4±0.6	29.9±0.8	32.3±0.5
In-Ir	15.0±0.7	16.9±0.3	16.3±0.4	15.5±0.2
CDDP	8.8±0.2	7.6±0.8	8.0±0.9	6.1±0.1

Fig. 2 Chemical structure, synthetic route and anti-tumor performance of **In-Ru**. (A) Chemical structure and synthetic route of **In-Ru**. (B and C) Intracellular Ru/Ir uptake and metal distribution in HepG2 cells after exposure for 8 h to Ppy-Ru/Ppy-Ir/**In-Ru**/**In-Ir**, as measured by ICP-MS. (D) TDO protein expression levels in different cell lines (HepG2, A549, HeLa). (E) IC_{50} (μM) values of Indo, Ppy-Ru, Ppy-Ir, **In-Ru**, **In-Ir** and CDDP toward different cell lines after treated for 48 h. Error bars: S.D., $n = 3$. $^{**}p < 0.01$, $^{***}p < 0.001$, $^{****}p < 0.0001$.

reference to previously reported literature.[35] After the metal precursors (Ppy-Ru, Ppy-Ir) were dissolved and reacted with $AgNO_3$ to remove Cl atom in methanol solution, the ligand Indo was added to the filtrate to form the final mononuclear complex **In-Ru** or **In-Ir** (Fig. 2A and Scheme S1†). All complexes were characterized by ^{1}H and ^{13}C NMR spectroscopy, and electrospray ionization mass spectra (ESI-MS), as shown in Fig. S1–S8.† Indo acts as a monodentate ligand and coordinates with Ppy-Ru or Ppy-Ir *via* its N atom in the final mononuclear complex **In-Ru** or **In-Ir**, that is further confirmed by distinct ESI-MS peaks at 628.2 ($[M–H]^+$) for **In-Ru** or 720.3 ($[M–H]^+$) for **In-Ir**.

Stability, lipophilicity, and intracellular distribution

The stability of **In-Ru** and **In-Ir** in DMSO/H_2O solution (5% DMSO) was investigated by UV-vis spectroscopy respectively. The time-dependent spectra and ESI-MS analysis reveal that these complexes remain stable under physiological conditions. This is primarily attributed to the η^6-coordinated arene ligand moiety which stabilizes the oxidation state of the ruthenium metal cation. Additionally, the negligible changes in the UV-vis spectra provide further evidence of their structural stability (Fig. S9†).

Lipophilicity (Log $P_{o/w}$) constitutes one of the crucial parameters for assessing the cell membrane penetrating ability

of drugs. The Log $P_{o/w}$ values determined by the octanol–water method were 1.33 and 0.65 for **In-Ru** or **In-Ir**, respectively. In contrast to metal precursors and Indo ligand, a high degree of lipophilicity is conducive to the accumulation of metal drugs in cancer cells (Fig. S10†). A positive correlation exists between intracellular drug accumulation and lipophilicity, and the cellular uptake capacity and subcellular organelle distribution of metal drugs were further determined by inductively coupled plasma mass-spectrometry (ICP-MS). After co-incubation of different complexes with HepG2 cells for 6 h, the content of Ru or Ir within the cells was determined. The results indicated that the introduction of lipophilic ligand was conducive to enhancing the cellular uptake of metal drugs. In both the groups of **In-Ru** and **In-Ir**, the metal ion content was observed significant increase, with the Ru content reaching 0.124 ng μg^{-1} protein, which was in accordance with the previously reported lipophilic properties of the complexes (Fig. 2B).[19] The distinctive structural characteristics of metal complexes are capable of targeting various subcellular organelles, thereby influencing cell survival and development through diverse pathways and demonstrating their inherent pharmacological properties. As shown in Fig. 2C, over 70% of Ru or about 45% of Ir accumulated in the nucleus, which indicates that the involvement of mononuclear ligand has augmented the burden imposed by metal drugs on the nuclei of cancer cells, which might give rise to a treatment modality related to nuclear damage.

Anti-proliferative activity

The anti-proliferative activity of different compounds against human hepatocellular carcinoma (HepG2), human lung cancer (A549), human cervical epithelioid carcinoma (HeLa), and human lung fibroblast (HLF) cell lines was evaluated by the MTT assay. **In-Ru** and **In-Ir** demonstrate diverse degrees of antiproliferative activity against various cancer cell lines, with the most remarkable inhibition observed in hepatocellular carcinoma cells. By contrast, the cytotoxicity of metal precursors and Indo ligand is merely moderate or almost non-toxic (Fig. 2E). It is noteworthy that **In-Ru** displays outstanding anti-proliferative activity against diverse cancer cells, with the inhibitory effect (IC_{50} value) escalating in the following sequence: A549 (6.90 μM) < HeLa (6.80 μM) < HepG2 (3.64 μM). We used cisplatin (CDDP) as the reference compound. **In-Ru** demonstrated a stronger anti-proliferative effect compared to CDDP. At the same time, it showed lower toxicity to normal cell HLF, demonstrating that **In-Ru** has a more superior therapeutic index. We analyzed the expression levels of TDO protein across various cancer cell lines. Notably, HepG2 cells exhibited significantly higher TDO expression compared to A549 and HeLa cells (Fig. 2D). This finding correlates well with the observation that **In-Ru** demonstrated superior anti-proliferative activity specifically in HepG2 cells (Fig. 2D, E and S11†).[36] The above results indicate that the anti-tumor activity of **In-Ru** and **In-Ir** is closely related to two factors: first, they exhibit better efficacy against cancer cells with high TDO expression, and second, their activity is positively correlated with cellular uptake in cancer cells. Since demonstrates significantly higher cellular uptake compared to **In-Ir**, the anti-tumor activity of **In-Ru** is much better that of **In-Ir**. Remarkably, the anti-tumor effect of **In-Ru** against HepG2 cells with much high TDO expression is superior to that observed in the other two tumor cell lines with low TDO expression. Based on the cytotoxicity characteristics, **In-Ru** was selected for further studies on HepG2 cells, while **In-Ir** was used as a control complex in some experiments.

Cell necroptosis and DNA damage

Inhibition of TDO levels promotes an increase in intracellular ROS levels and impairs mitochondrial membrane potential, thereby triggering necroptosis in cancer cells.[37,38] RIP3 (receptor-interacting protein 3) and NF-κB (p65) (RelA, a subunit of NF-κB) play critical roles in this process, contributing to cell membrane rupture and the release of intracellular contents.[39] To examine cell death mechanism of **In-Ru**, different inhibitors for cell death modes were applied in HepG2 cells (Fig. S12†). After treated with different inhibitors, cells demonstrate diverse levels of viability. Neither Ferroptotic inhibitor Ferrostatin-1(Fer-1) nor autophagic inhibitor chloroquine (CQ) exerted a significant impact on cell viability. While after incubated with apoptotic inhibitor z-VAD-fmk and necrotic inhibitor Necrostatin-1 (Nec-1), cell viabilities were significantly improved, implying that **In-Ru** could induce cell death by necroptosis and apoptosis pathways. Additionally, the cell lethality treated with **In-Ru** was demonstrated by flow cytometry on HepG2 cells (Fig. 3A). With the concentration of **In-Ru** rose, the proportion of cell necroptosis rose linearly, far surpassing that of the other experimental groups. Even with complex concentration at 4 μM, it could induce approximately 27.1% of cell necroptosis. Subsequently, we investigated the changes in these related proteins. Upon co-incubation with **In-Ru**, RIP3 expression was upregulated by more than 7-fold, which strongly confirmed the occurrence of necroptosis in HepG2 cells. Additionally, we assessed the expression changes of p65 protein in HepG2 cells and found that after treatment with **In-Ru**, the p65 content decreased to approximately one-third of that in the control group (Fig. 3B and C). From the bright-field microscopic images, it is evident that treatment with **In-Ru** induces necroptosis in cells, leading to cell membrane disruption and the release of antigenic substance (Fig. 3D). These results indicate that **In-Ru** can induce necroptosis in HepG2 cells by suppressing TDO expression, thereby potentially enhancing the anti-tumor efficacy of the complex.

ROS generation and mitochondrial membrane potential ($\Delta\Psi_m$)

Cell necroptosis typically related to the disruption of the cellular oxidative-reduction homeostasis and impairment of mitochondrial function membrane potential ($\Delta\Psi_m$, MMP).[40] Flow cytometry results indicated that ROS gradually accumulated in cells treated with diverse compound groups, with **In-Ru** at 8 μM eliciting a significant increase in ROS concentration, approximately five-fold that of the control group. The bright green fluorescence signal in confocal laser scanning microscope (CLSM) images likewise attests to the capacity of **In-Ru** to

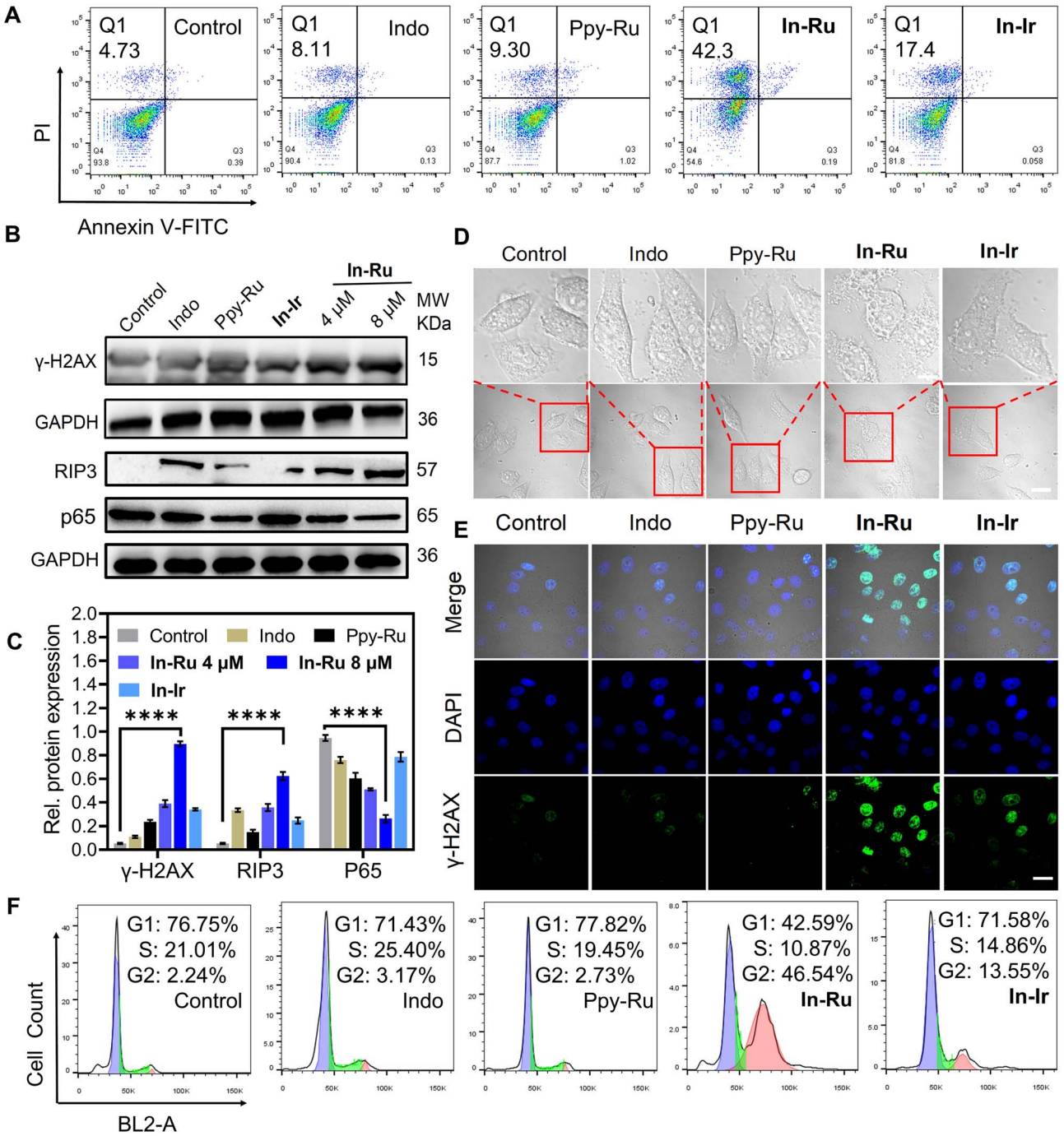

Fig. 3 Investigation into the mechanism of necroptosis and DNA damage in HepG2 cells induced by **In-Ru**. (A) Flow cytometry analysis of apoptosis and necroptosis evaluation treated with different compounds for 24 h by Annexin-FITC and PI assay. (B) Western blot analysis of the expression of DNA damage (γ-H2AX) and necroptosis (RIP3, p65) proteins treated with different compounds for 24 h. (C) Quantitative analysis for expressions of γ-H2AX, RIP3 and p65 proteins in (B). (D) Representative bright-field images of HepG2 cells treated with various compounds for 24 h are shown. **In-Ru** can induce cell necroptosis and promote antigen release. Scale bar: 20 μm. (E) Immunofluorescence images of HepG2 cells indicating the signal of γ-H2AX after incubation with Indo, Ppy-Ru, Ppy-Ir, **In-Ru**, **In-Ir** for 24 h. Scale bar: 20 μm. γ-H2AX antibody: λ_{ex} = 488 nm, λ_{em} = 525 ± 20 nm; DAPI: λ_{ex} = 405 nm, λ_{em} = 430 ± 20 nm. (F) Cell cycle arrest of HepG2 cells after incubation with different compounds at the same concentration for 24 h. Error bars: S.D., n = 3. *p < 0.05, **p < 0.01, ***p < 0.001, ****p < 0.001.

induce ROS production (Fig. S13†). The effect of **In-Ru** on the $\Delta\Psi_m$ of HepG2 cells was tested using the JC-1 (5,5′,6,6′-tetrachloro-1,1′,3,3′-tetraethylbenzimi-dazolylcarbocyanine iodide) assay kit. The alterations in $\Delta\Psi_m$ were manifested by the increase of green fluorescence (JC-1 monomers) and the decrease of red fluorescence (JC-1 aggregates). Upon treatment of the cells with the different compounds, the red signal attenuated in these groups, concurrently with the emergence of the green signal. When **In-Ru** was introduced, the green fluorescence was conspicuously enhanced, while the red

fluorescence almost vanished (Fig. S14†). The flow cytometry analysis indicated that 65% of the cells subjected to **In-Ru** displayed high JC-1 monomers signals, in contrast to 0.5% of the control cells. Overall, **Indo-Ru** significantly enhanced ROS levels, which might induce DNA and mitochondrial damage in cancer cells and ultimately result in cell apoptosis and necroptosis.

Considering that **In-Ru** accumulates in the nucleus of cells in considerable quantities and is capable of inducing cell death through necroptosis and other pathways, the cytotoxicity of the complex might be triggered by nuclear damage and mediate cell apoptosis and necroptosis. The nucleus houses the genomic materials, regulates gene expression, and governs the replication of DNA during the cell cycle. DNA damage within the nucleus is succeeded by the phosphorylation of histone H2AX in recruiting and localizing the proteins for DNA damage repair. Thus, the expression of γ-H2AX in HepG2 cells was evaluated by western blotting to disclose the function of metal complexes in inducing DNA damage. As shown in Fig. 3B and C, **In-Ru** elicited a marked upregulation of γ-H2AX during 24 h, which indicated that complex could induce DNA damage. Nevertheless, **In-Ir** demonstrates a relatively low potential for DNA damage, which might be associated with its relatively low cellular uptake. Meanwhile, CLSM imaging was utilized to further substantiate the occurrence of DNA damage. In contrast to the control group and other compounds, the green fluorescence of γ-H2AX within the cells treated with **In-Ru** was markedly enhanced, disclosing the occurrence of DNA damage pattern (Fig. 3E). Cellular DNA damage could induce cell cycle arrest.[41] Cell division cycles in HepG2 cells during treatment were recorded by flow cytometry after incubation with different compounds for 24 h. A negligible alteration in cell cycle distribution was detected in the control group. However, the G2 arrest was witnessed significantly after treatment with **In-Ru**, with the proportion of the G2 phase was increased by 44% compared to the control group (Fig. 3F). This indicates that **In-Ru** upregulates the expression of γ-H2AX protein and induces severe DNA damage, resulting in G2 arrest in HepG2 cells.

Autophagy

Autophagy plays a critical role in maintaining intracellular homeostasis, and the elevation of ROS levels can promote autophagy induction.[42] We assessed the ability of **In-Ru** to induce autophagy using immunofluorescence imaging and western blot analysis. As shown in Fig. S15,† compared with the control group and other compound-treated groups, cells treated with **In-Ru** exhibited significantly enhanced green fluorescence signals corresponding to LC3 protein, indicating that **In-Ru** induces autophagosome formation. Furthermore, the western blot results confirmed these findings by demonstrating increased expression levels of LC3-II and decreased levels of p62, which are hallmarks of autophagy activation.

RNA-sequence (seq) analysis

To further illuminate the specific anti-tumor mechanisms and the enhancement effect mediated by TDO inhibition of **In-Ru**, RNA-seq analysis was conducted on HepG2 cells treated with the complex for 24 h. As indicated in Table S2,† the proportion of ribosomal RNA is less than 5%, while the percentage of uniquely mapped reads exceeds 90%, aligning with the standard threshold (>70%). The average sequencing coverages for the control and **In-Ru** group is 94.53% and 93.62%, respectively. The correlation coefficient between replicate samples exceeds 0.747, and over 80% of the mapped reads are located within exonic regions. These findings confirm the reproducibility and reliability of the observed significant differences between the control and **In-Ru** group in the downstream analysis. Fig. 4A presents a volcano plot of 761 significantly differentially expressed genes (DEGs) between the **In-Ru** group and the control group, with $|\log_2 FC| > 1$. Among these, 328 genes were upregulated and 433 genes were downregulated. Kyoto Encyclopedia of Genes and Genomes (KEGG) enrichment analysis revealed that **In-Ru** can modulate the tryptophan metabolic pathway, IL-17 signaling pathway, and NF-κB signaling pathway, TNF signaling pathway, and natural killer cell-mediated cytotoxicity (Fig. 4B). GO enrichment analysis further demonstrated that **In-Ru** effectively promotes the regulation of inflammatory responses, tryptophan metabolism, and activates immune therapy-related pathways through TDO inhibition (Fig. S16†). Additionally, **In-Ru** influences aryl hydrocarbon receptor signaling in the tryptophan metabolic pathway, negatively regulates gene expression, modulates T cell antigen processing and presentation, mediates metal ion binding in the nucleus and cytoplasm, facilitates DNA binding, and enhances the activity of DNA-binding transcription factors (Fig. S17 and 18†).

Treatment with **In-Ru** resulted in significant alterations in the tryptophan metabolic pathway within cells, which facilitates the reversal of immunosuppression and activation of T cells *via* the TDO pathway.[25] Gene set enrichment analysis (GSEA) reveals that variations in gene expression are significantly correlated with TDO downregulation and immune signaling pathways (Fig. 4D and S19†). Furthermore, immune-related genes involved in innate and adaptive immune responses, including the T-cell receptor signaling pathway, TNF signaling pathway, NF-κB signaling pathway, and IL-17 signaling pathway,[43,44] were significantly upregulated. Subsequently, a detailed analysis of the related genes in each pathway was conducted. Specifically, we examined genes associated with the TDO pathway (Fig. 4E). As expected, inhibitory genes such as KYN, DHTDK1, DLD, ACAT1, AOX1, KYAT3 were significantly downregulated, consistent with the negative regulation observed in the GSEA results.[45–48] Additionally, the upregulation of immune-related genes (IL-6, IFN-β, TNF-α, NF-κB, and LIF) further confirmed an enhanced immune response in cells following **In-Ru** treatment. Significant changes in necroptosis-related genes (RNF103-CHMP3,[49] HSP90AA1, FTL, BCL2, RIPK1)[50] provided strong evidence of cell death. Collectively, these data suggest that **In-Ru** can enhance both innate and adaptive immunity by activating HepG2 cells through TDO pathway, thereby promoting an anti-tumor immune response.

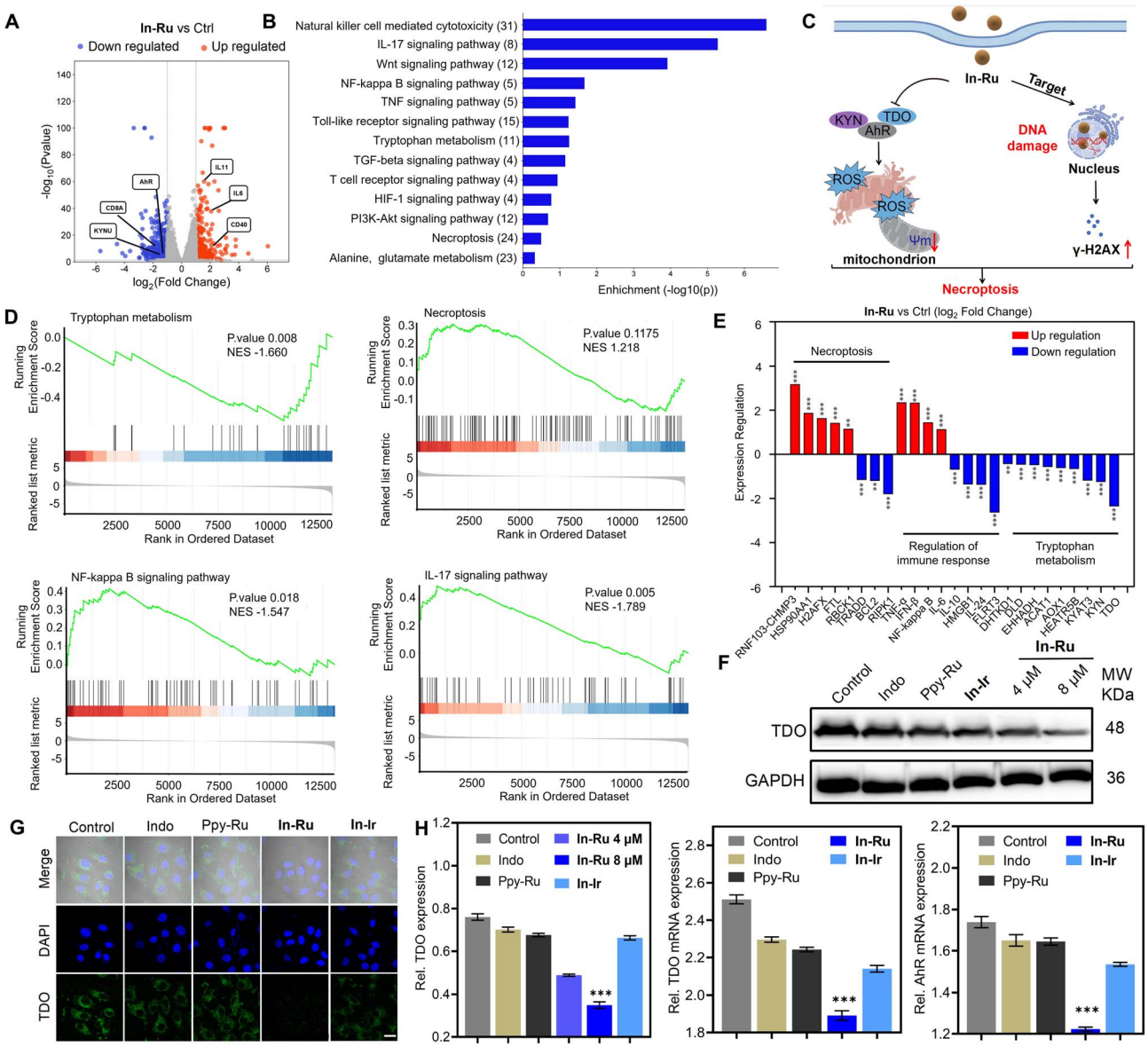

Fig. 4 Assessment of TDO inhibition and ICD-induced immune activation. (A) Volcano plot showing the DEGs in HepG2 cells treated with **In-Ru** (4 μM) for 24 h. Standard: $|\log_2 FC| > 1$; q-value <0.05. (B) KEGG enrichment analysis of differentially expressed genes after treated by **In-Ru** (4 μM) for 24 h. (C) **In-Ru** molecule targets the cell nucleus, inducing DNA damage while simultaneously suppressing the expression of TDO. These combined effects lead to necroptosis in HepG2 cells. (D) GSEA reveals negative and positive enrichment of altered genes in cellular processes after treated by **In-Ru** (4 μM) for 24 h. Standard: observed genes > 2, fold change > 2 and FDR < 0.05 (Tryptophan metabolism, Necroptosis, NF-κB signaling pathway, IL-17 signaling pathway). (E) Expression level changes of the impacted genes involved in necroptosis, regulation of immune response and tryptophan metabolism in HepG2 cells treated with **In-Ru**. (F) Western blot analysis of TDO inhibition in HepG2 cells treated with various compounds for 24 h. (G) Confocal images of TDO signal in HepG2 cells treated with various compounds for 24 h. FITC: $\lambda_{ex} = 488$ nm, $\lambda_{em} = 525 \pm 20$ nm; DAPI: $\lambda_{ex} = 364$ nm, $\lambda_{em} = 454 \pm 20$ nm. Scale bar: 20 μm. (H) Quantitative analysis for expressions of TDO proteins in (F); statistical analysis of TDO and AhR mRNA expression changes following treatment with various compounds. Error bars: S.D., $n = 3$. *$p < 0.05$, **$p < 0.01$, ***$p < 0.001$, ****$p < 0.001$.

Modulation of TDO and AhR signaling proteins

TDO is an enzyme that overexpressed in liver cancer tissues and functions as a critical species in the regulation of the activation of the aryl hydrocarbon receptor (AhR) and tumor immune escape.[46] Thus, in light of the TDO inhibitory mechanism of Indo, we further examined the mechanism of **In-Ru** in the TDO immune response. Similar to other immune checkpoint inhibitors, suppressing the levels of TDO is conducive to facilitating the activation and proliferation of T cells, thereby strengthening the anti-tumor immune response.[33] Then the ability of **In-Ru** to inhibit TDO protein expression in HepG2 cells was examined. As shown in Fig. 4F, after treated with **In-Ru**, the expression of TDO in the cells was significantly downregulated and demonstrated a dependence on the complex concentration, but that in the other treatment groups exhibited a more

moderate trend, with no significant differences in alterations (Fig. 4F). The CLSM images (Fig. 4G) revealed more intense TDO-associated fluorescence signals in the control group, which completely disappeared following **In-Ru** treatment, indicating substantial suppression of TDO activity. In contrast, fluorescence signals for TDO exhibited varying degrees of attenuation after exposure to the other tested compounds. To further investigate the mechanism of **In-Ru** *via* the TDO pathway, we evaluated the expression of TDO and AhR through quantitative reverse transcriptase polymerase chain reaction (qRT-PCR) in HepG2 cells (Fig. 4H). Following incubation with **In-Ru**, the mRNA levels of TDO and AhR in cells were significantly reduced by approximately 24% or 30%, respectively, demonstrating inhibitory effects that were markedly stronger than those of other compounds (Fig. 4H and S20†). **In-Ru** could induce nuclear damage which further impede the accumulation of AhR in the nucleus and diminish its expression. The results suggest that **In-Ru**, as a novel TDO immune checkpoint inhibitor, is capable of inhibiting the expression of TDO protein and mediating the inactivation of the downstream AhR pathway to obstruct the TDO-AhR signaling pathway.

ICD effect *in vitro*

In-Ru accumulates abundantly in the nucleus of cells and can induce necroptosis in liver cancer cells, which might evoke a potent immunogenicity.[51] Considering the immune response elicited by **In-Ru** and the reversal of immune suppression, we subsequently assessed the efficacy of the TDO inhibitor based on the MLSE strategy against ICD, which were further investigated in HepG2 cells. ICD possesses three key signals, including high mobility group box-1 protein (HMGB1) release, adenosine

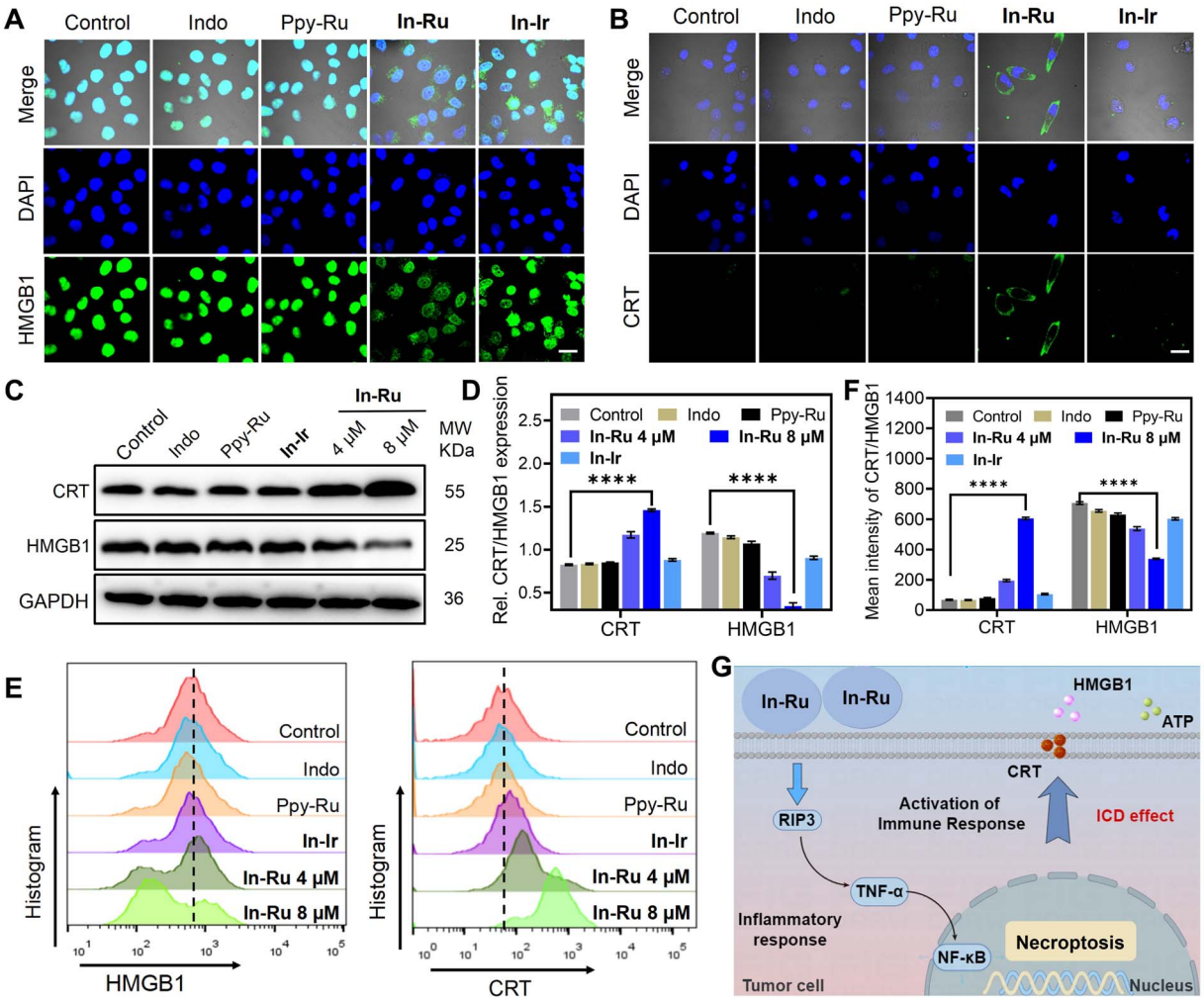

Fig. 5 Detection and analysis of ICD marker signals in HepG2 cells treated by **In-Ru**. (A) Confocal images of HMGB1 release in HepG2 cells incubated with various compounds for 24 h (Indo, Ppy-Ru, **In-Ru**, **In-Ir**). Scale bar: 20 μm. HMGB1 antibody: $\lambda_{ex} = 488$ nm, $\lambda_{em} = 520 \pm 20$ nm; DAPI: $\lambda_{ex} = 405$ nm, $\lambda_{em} = 430 \pm 20$ nm. (B) Confocal images of CRT release in HepG2 cells incubated with various compounds for 24 h (Indo, Ppy-Ru, **In-Ru**, **In-Ir**). Scale bar: 20 μm. CRT antibody: $\lambda_{ex} = 488$ nm, $\lambda_{em} = 520 \pm 20$ nm; DAPI: $\lambda_{ex} = 405$ nm, $\lambda_{em} = 430 \pm 20$ nm. (C) Western blot analysis for the expression of CRT and HMGB1 proteins in HepG2 cells treated with Indo, Ppy-Ru, **In-Ru**, **In-Ir** for 24 h. (D) Quantitative analysis for expressions of CRT/HMGB1 proteins in (C). (E) Flow cytometry analysis of HMGB1 and CRT expression changes evaluation treated with different compounds for 24 h. (F) Quantitative analysis of CRT/HMGB1 intensity changes in (E). (G) Induction of ICD and associated immune responses by cell necroptosis. Error bars: S.D., $n = 3$. *$P < 0.05$, **$P < 0.01$, ***$P < 0.001$, ****$P < 0.001$.

triphosphate (ATP) secretion and calreticulin (CRT) exposure.[14] As shown in Fig. 5A, the stimulation of **In-Ru** induced a decrease in HMGB1 expression in the nucleus as detected by CLSM images. Typically, HMGB1 is retained within the nucleus of normal cells, but released into the extracellular space in necrotic cells. The assay of intracellular HMGB1 by western blot and flow cytometry indicated that **In-Ru** caused the greatest leakage of HMGB1 compared to other groups (Fig. 5C–E), which also in accordance with the fact that **In-Ru** induces the most severe cell necroptosis. Furthermore, green strong emission signals of CRT antibody of the whole cell, excluding the nucleus, suggested its exposure after treated by **In-Ru**. Flow cytometry analysis indicated a dose-dependent increase of CRT level in the **In-Ru** group. Inducing ICD typically results in the substantial release of ATP from the cells. ATP release was detected by the ATP detection kit, the results demonstrate that **In-Ru** significantly promotes ATP secretion in a dose-dependent manner. Additionally, the marked decrease in intracellular ATP levels corroborates the release of ATP from the cytoplasm into the extracellular space (Fig. S21†). The experiment results demonstrate that **In-Ru** accumulates extensively in the cell nucleus, inducing robust necroptosis and promoting intracellular substance leakage, thereby significantly enhancing anti-tumor immunity. In contrast, at the same concentration, the ligand Indo and metal precursor Ppy-Ru exhibit limited cellular uptake and low anti-tumor activity, failing to induce effective ICD effect. Furthermore, inhibition of TDO expression directly promotes ROS generation and impairs mitochondrial function, thereby triggering more pronounced necroptosis. This novel metal complex not only enhances cytotoxicity but also effectively triggers ICD, achieving immunotherapeutic effects at low doses, thus facilitating further investigation into *in vivo* immune activation mechanisms.

Biological evaluation on 3D multicellular tumor spheroids

In preclinical basic research, 3D multicellular tumor spheroids (MCTSs) used as the widely utilized tumor model, were employed to assess the biological anti-proliferative effects of **In-Ru**. Compared to cultured cell lines, solid tumor models exhibit reduced sensitivity to chemotherapeutic drugs and can effectively simulate the microenvironment of solid tumors.[52] The morphology and growth of 3D MCTSs were assessed every 48 h over a period of 8 days. As shown in Fig. 6A and B, the MCTS in the **In-Ru** group began to shrink in volume after 2 days of treatment. By the end of 8 days after treatment, the spheroids became loose and their boundaries disappeared, indicating that the **In-Ru** had severely affected the morphological growth and integrity of the MCTS. In the absence of drug intervention, the tumor spheres naturally grew to a diameter of approximately 600 μm and had a volume approximately four times that of the **In-Ru** treatment group. After incubation with **In-Ir**, the spheroids exhibited nearly complete growth arrest, demonstrating

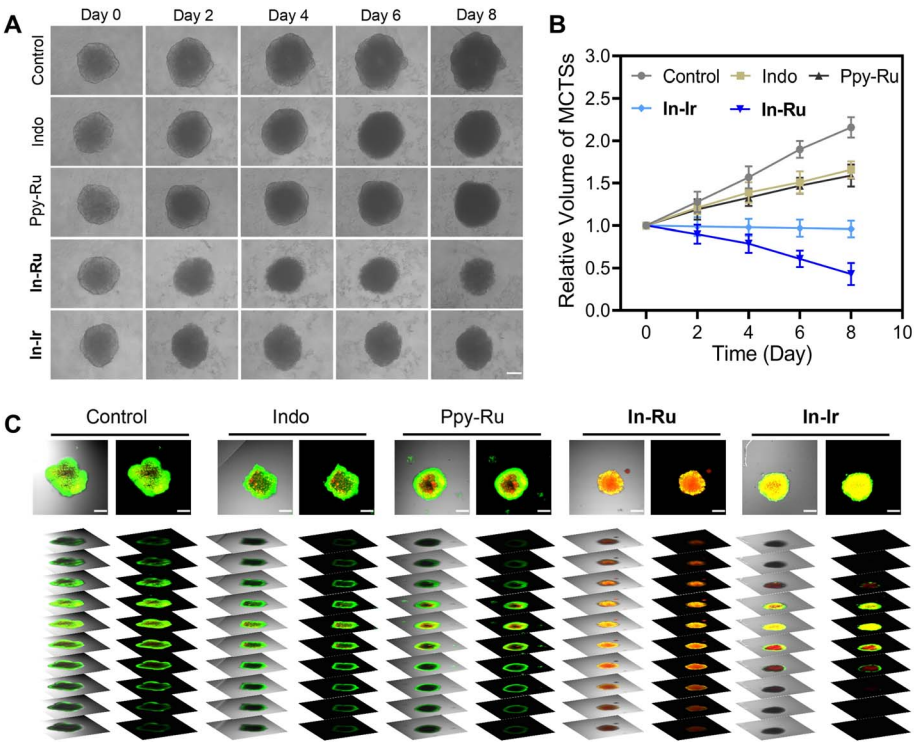

Fig. 6 Evaluation of the cytotoxicity and anti-tumor activity of **In-Ru** on 3D HepG2 tumor cell spheroids. (A) Representative images of 3D tumor spheroids treated with various compounds every 48 h for 8 days, Indo (30 μM), Ppy-Ru (30 μM), **In-Ru** (30 μM), **In-Ir** (30 μM). Scale bar: 200 μm. (B) Curves of 3D tumor spheroids volume treated with PBS, Indo, Ppy-Ru, **In-Ru** and **In-Ir**. (C) Confocal images of the live/dead cells in the tumor spheroids after treatment with PBS, Indo, Ppy-Ru, **In-Ru** and **In-Ir** for 8 days, stained by Calcein AM/PI and photographed by confocal microscope. Scale bar: 200 μm. Error bars: S.D., $n = 3$.

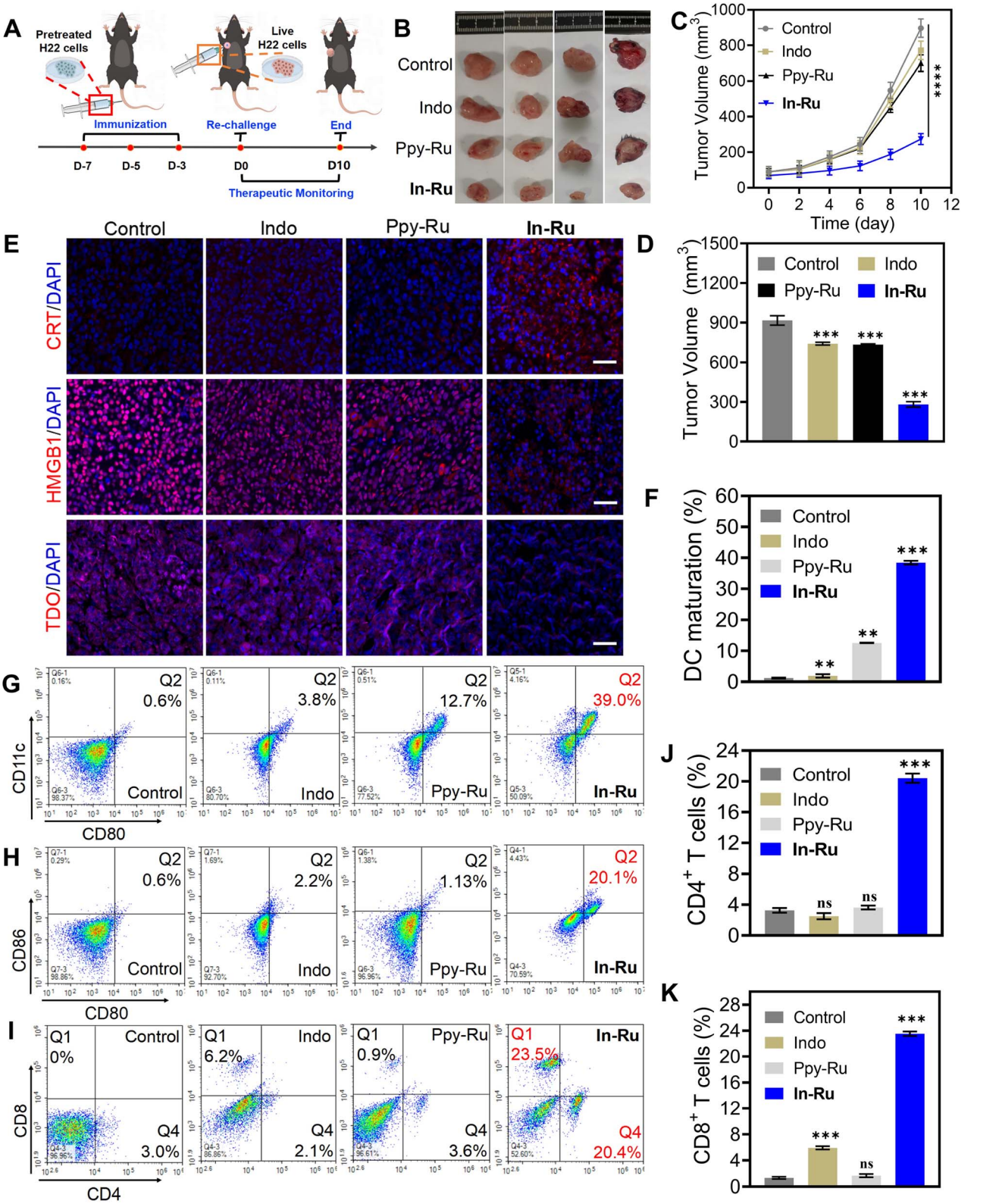

Fig. 7 Vaccine administration and tumor suppression. (A) Schematic diagram of the vaccine administration experiment workflow. (B) Representative photographs of dissected tumors with various treatment conditions for 10 days as illustrated in (A). (C) Curves of H22 tumor volume treated with PBS, Indo, Ppy-Ru and **In-Ru**. (D) Tumor weight on day 10 in the various treatment groups. (E) Immunofluorescence analysis of specific protein expression (CRT, HMGB1 and TDO) from primary tumor tissues *via* staining with the corresponding probes. Scale bar: 200 μm. (F–H) Flow cytometry of DC maturation by determining $CD11c^+$ $CD80^+$ $CD86^+$ cells in primary tumors. (I–K) The proportion of primary tumor infiltrating T lymphocytes ($CD8^+$ and $CD4^+$) measured with different treatments by flow cytometry. Error bars: S.D., $n = 4$. *$p < 0.05$, **$p < 0.01$, ***$p < 0.001$, ****$p < 0.001$.

a certain degree of anti-proliferative activity. To further elucidate the impact of **In-Ru** on cell viability within MCTS, a dual-staining approach utilizing calcein AM (green fluorescence) for live cells and propidium iodide (red fluorescence) for dead cells was employed. In the control group, bright green fluorescence indicated that most cells were alive, while weak red signals representing cell death were observed in several treatment groups. In the MCTS treated with **In-Ru**, the strong red fluorescence signal indicated irreversible damage to the spheres and cell death (Fig. 6C). These results indicate that **In-Ru** not only demonstrated superior tumor penetration ability but also effectively inhibited the proliferation of HepG2 3D MCTSs compared to the control group.

Activation of anti-tumor immunity *in vivo*

In-Ru can inhibit TDO expression in HepG2 cells and enhance the efficacy of immunotherapy. We further evaluated the potential of the complex in mediating TDO inhibition and immunotherapy *in vivo* through mouse vaccination experiments.[14] As illustrated in Fig. 7A, healthy C57BL/6J mice received intravenous injections of H22 hepatocellular carcinoma cells, which had undergone various treatments (PBS, Indo, Ppy-Ru, **In-Ru**) on days −7, −5, and −3. Then, on day 0, 1×10^6 viable H22 cells were subcutaneously inoculated into each mouse, and tumor volume and body weight were monitored every two days over a period of 10 days. Analysis of the tumor growth trend in mice showed that the tumor growth in mice immunized with **In-Ru**-treated H22 cells was significantly inhibited, while in the other groups, the tumor growth rate showed a phased upward trend (Fig. 7B–D and S22†). Hematoxylin-eosin (H&E) staining analysis of tumor sections also showed large number of dead cells in group treated with **In-Ru**-treated H22 cells. Meanwhile, no significant changes were observed in body weight or major organ morphology across all groups of mice during the treatment period indicates the safety and stability of the therapeutic agents and vaccine regimens (Fig. S23†). **In-Ru** can inhibit TDO *in vitro*, which subsequently results in the down-regulation of AhR expression. We performed a series of *in vivo* experiments to determine whether the observed effects *in vitro* could be replicated within a living organism. Immunofluorescence staining analysis of tumor sites in mice revealed that, the fluorescence signal intensities of HMGB1 and TDO compared to the PBS group, were reduced by 4.5- and 2.4-fold after treatment, respectively (Fig. S24†). Compared with the reported platinum-based TDO inhibitor, **In-Ru** exhibits a more pronounced inhibitory effect on TDO.[33] Concurrently, CRT signaling was significantly enhanced (Fig. 7E). These findings collectively demonstrate the capacity of **In-Ru** to suppress TDO expression and induce ICD activation *in vivo*.

The dead tumor cells caused by ICD effect, leading to the release of associated antigenic substances.[53] This process subsequently stimulates various types of immune cells and ultimately promotes systemic immune activation.[54] DCs as the primary antigen-presenting cells, play a crucial role in mediating communication between the innate and adaptive immune systems. ICD-induced tumor-associated substances promote the maturation of DCs. Subsequently, these antigens are captured by mature DCs and presented specifically to T cells, triggering a cellular immune response against homologous cancers. The increased proportion of $CD80^+$ $CD86^+$ cells, a hallmark of DCs maturation, rose from 0.6% to 20% in the tumor microenvironment of treated mice, which facilitated robust activation of adaptive immunity (Fig. 7F–H). Cytotoxic T lymphocytes (CTLs, $CD3^+$ $CD4^+$ $CD8^+$) play a crucial role in tumor cytotoxicity and immune defense, while $CD8^+$ T cells serve as the direct indicator of autoimmune activation and tumor killing.[55] As shown in Fig. 7I–K, the percentage of $CD8^+$ T cells increased approximately 20-fold compared to the untreated group. Notably, **In-Ru** demonstrated a more pronounced enhancement in $CD8^+$ T cell activation, showing superior activation ratios compared to other ruthenium-based complexes (**RuBTB:** (≈3.9 fold); **6a**: (≈2.0 fold); Ru2c@biotin-DNA cage: (≈1.5 fold)).[19,56,57] Meanwhile, Ppy-Ru failed to promote T cell activation, whereas the TDO inhibitor Indo significantly increased the proportion of T cells, likely due to its ability to reverse the immunosuppressive microenvironment. $CD4^+$ T cells possess the ability to assist $CD8^+$ T cells in performing immune functions and participating in immune responses. The proportion of $CD4^+$ T cells in **In-Ru** group increased approximately 6.5-fold, the value from 3% to 20.3%. Remarkably, **In-Ru** exhibited markedly superior enhancement in $CD4^+$ T cell activation compared to other ruthenium complexes (**RuBTB:** (≈5.4 fold); Ru2c@biotin-DNA cage: (≈1.5 fold)).[56,57] **In-Ru** serves as an effective immunomodulator by inhibiting TDO to suppress kynurenine production, thereby reversing the immunosuppressive microenvironment in tumor tissues and enhancing the activation and proliferation of T cells. These critical results demonstrate that **In-Ru** can effectively ablate tumors *in vivo* and robustly activate the potent anti-tumor immune response through the synergistic effects of chemotherapy and immunotherapy, highlighting the potential of MLSE strategy in the treatment of solid tumors.

Conclusions

In conclusion, this study developed a Ru(II)-arene anti-tumor complex (**In-Ru**) that effectively inhibits TDO expression, thereby inducing ICD effect and reshaping the tumor immune microenvironment. **In-Ru** mediates the TDO/KYN/AhR metabolic pathway to alleviate tryptophan depletion, modulate the immune microenvironment, and promote T-cell proliferation and infiltration. Furthermore, **In-Ru** exhibits nuclear targeting properties, inducing severe DNA damage and thereby triggering necroptosis. This resulted in cell membrane rupture and antigen release, eliciting a systemic immune response. The *in vivo* vaccine experiments demonstrated that **In-Ru** effectively reduces TDO levels in solid tumors, activates the ICD effect, and enhances T cell-mediated immune cytotoxicity. This MLSE-based approach enables precise coordination between immune checkpoint inhibitors and metal-arene precursors, establishing a dual mechanism that synergistically augments chemotherapeutic and immunotherapeutic efficacy while

concurrently diminishing therapeutic agent dosage requirements, thereby effectively mitigating associated adverse events. This paradigm not only systematically elucidates the anti-tumor immune mechanisms of metal-based TDO inhibitors but also offers new perspectives for developing safe and effective metal-based immunotherapies.

Ethical statement

All animal procedures were performed in accordance with the Guidelines for Care and Use of Laboratory Animals of "Nanjing Normal" University and approved by the Animal Ethics Committee of "Nanjing Normal University".

Data availability

The data that support the findings of this study are available in the ESI of this article.†

Author contributions

Zheng-Qi Shen: writing – original draft, validation, methodology, investigation, formal analysis. Binglian Guo: methodology, formal analysis. Xiangyu Dai: formal analysis, data curation. Hanxue Liu: resources, methodology. Meng Ren: writing – review & editing, visualization. Peisen Wang: methodology, writing – review & editing, visualization. Yating Zhang: resources, formal analysis. Yinuo Xu: resources, formal analysis. Zhi Su: validation. Xuling Xue: writing – review & editing, visualization, resources. Hongke Liu: writing – review & editing, supervision, resources, funding acquisition, conceptualization.

Conflicts of interest

The authors declare no conflict of interest.

Acknowledgements

This work was financially supported by the National Natural Science Foundation of China (No. 22077066, No. 22477062), Original Exploration Program of National Natural Science Foundation of China (No. 22350001) and the Postgraduate Research & Practice Innovation Program of Jiangsu Province (KYCX24-1805).

References

1 X. Wang, X. Wang, S. Jin, N. Muhammad and Z. Guo, *Chem. Rev.*, 2019, **119**, 1138–1192.
2 Q. Fu, S. Zhang, S. Shen, Z. Gu, J. Chen, D. Song, P. Sun, C. Wang, Z. Guo, Y. Xiao, Y. Q. Gao, Z. Guo and Z. Liu, *Nat. Biomed. Eng.*, 2024, **8**, 1425–1435.
3 H.-K. Liu and P. J. Sadler, *Acc. Chem. Res.*, 2011, **44**, 349–359.
4 N. P. E. Barry and P. J. Sadler, *Chem. Soc. Rev.*, 2012, **41**, 3264.
5 Z. Liu and P. J. Sadler, *Acc. Chem. Res.*, 2014, **47**, 1174–1185.
6 J. Shen, T. W. Rees, L. Ji and H. Chao, *Coord. Chem. Rev.*, 2021, **443**, 214016.
7 K. Peng, Y. Zheng, W. Xia and Z.-W. Mao, *Chem. Soc. Rev.*, 2023, **52**, 2790–2832.
8 C. Zhang, N. Montesdeoca, S. Tang, H. Liang, H. Cui, C. Xu, L. M. Servos, J. Bing, Z. Papadopoulos, F. Shen, H. Xiao, J. Yu and J. Karges, *Nat. Commun.*, 2024, **15**, 9405.
9 S. Sen, S. Hufnagel, E. Y. Maier, I. Aguilar, J. Selvakumar, J. E. DeVore, V. M. Lynch, K. Arumugam, J. L. Sessler and J. F. Arambula, *J. Am. Chem. Soc.*, 2020, **142**, 20536–20541.
10 K. Shang, N. Montesdeoca, C. Zhang, E. Efanova, H. Liang, J. Ochs, J. karges, Q. Song and P. Zhang, *J. Controlled Release*, 2024, **373**, 496–506.
11 P. Kaur, A. Johnson, X. Lu and K. Suntharalingam, *ChemBioChem*, 2020, **21**, 3618–3624.
12 J. P. C. Coverdale, I. Romero-Canelón, C. Sanchez-Cano, G. J. Clarkson, A. Habtemariam, M. Wills and P. J. Sadler, *Nat. Chem.*, 2018, **10**, 347–354.
13 L. Zeng, P. Gupta, Y. Chen, E. Wang, L. Ji, H. Chao and Z.-S. Chen, *Chem. Soc. Rev.*, 2017, **46**, 5771–5804.
14 M. Lv, Y. Zheng, J. Wu, Z. Shen, B. Guo, G. Hu, Y. Huang, J. Zhao, Y. Qian, Z. Su, C. Wu, X. Xue, H. Liu and Z. Mao, *Angew. Chem., Int. Ed.*, 2023, **62**, e202312897.
15 X. Xue, C. Qian, H. Fang, H. Liu, H. Yuan, Z. Guo, Y. Bai and W. He, *Angew. Chem., Int. Ed.*, 2019, **58**, 12661–12666.
16 H. Liu, S. J. Berners-Price, F. Wang, J. A. Parkinson, J. Xu, J. Bella and P. J. Sadler, *Angew. Chem., Int. Ed.*, 2006, **45**, 8153–8156.
17 X. Xue, C. Qian, Q. Tao, Y. Dai, M. Lv, J. Dong, Z. Su, Y. Qian, J. Zhao, H.-K. Liu and Z. Guo, *Natl. Sci. Rev.*, 2021, **8**, nwaa286.
18 H.-K. Liu, J. A. Parkinson, J. Bella, F. Wang and P. J. Sadler, *Chem. Sci.*, 2010, **1**, 258.
19 M. Lv, Y. Zheng, X. Dai, J. Zhao, G. Hu, M. Ren, Z. Shen, Z. Su, C. Wu, H.-K. Liu, X. Xue and Z.-W. Mao, *J. Med. Chem.*, 2024, **67**, 20156–20171.
20 M. Wang, F. Xu, Y. Su, Y. Geng, X. Qian, X. Xue, Y. Kong, Z. Yu, H. Liu and Z. Su, *Angew. Chem., Int. Ed.*, 2022, **61**, e202203843.
21 N. Xu, G.-D. Zhang, Z.-Y. Xue, M.-M. Wang, Y. Su, H. Fang, Z.-H. Yu, H.-K. Liu, H. Lu and Z. Su, *Chem. Eng. J.*, 2024, **497**, 155022.
22 P. Wang, H. Fang, M. Wang, G. Zhang, N. Xu, Y. Su, H. Liu and Z. Su, *Chin. Chem. Lett.*, 2025, **36**, 110099.
23 C. Lu, D. Rong, B. Zhang, W. Zheng, X. Wang, Z. Chen and W. Tang, *Mol. Cancer*, 2019, **18**, 130.
24 J. Zheng, S. Wang, L. Xia, Z. Sun, K. M. Chan, R. Bernards, W. Qin, J. Chen, Q. Xia and H. Jin, *Signal Transduct. Targeted Ther.*, 2025, **10**, 35.
25 J. E. Cheong and L. Sun, *Trends Pharmacol. Sci.*, 2018, **39**, 307–325.
26 S. I. Ilyas, J. Wang and A. B. El-Khoueiry, *Hepatology*, 2021, **73**, 86–103.
27 Y. Liu, X. Liang, W. Dong, Y. Fang, J. Lv, T. Zhang, R. Fiskesund, J. Xie, J. Liu, X. Yin, X. Jin, D. Chen, K. Tang, J. Ma, H. Zhang, J. Yu, J. Yan, H. Liang, S. Mo, F. Cheng, Y. Zhou, H. Zhang, J. Wang, J. Li, Y. Chen, B. Cui, Z.-W. Hu, X. Cao, F. Xiao-Feng Qin and B. Huang, *Cancer Cell*, 2018, **33**, 480–494.

28 C. A. Opitz, U. M. Litzenburger, F. Sahm, M. Ott, I. Tritschler, S. Trump, T. Schumacher, L. Jestaedt, D. Schrenk, M. Weller, M. Jugold, G. J. Guillemin, C. L. Miller, C. Lutz, B. Radlwimmer, I. Lehmann, A. Von Deimling, W. Wick and M. Platten, *Nature*, 2011, **478**, 197–203.
29 J. Yan, D. Chen, Z. Ye, X. Zhu, X. Li, H. Jiao, M. Duan, C. Zhang, J. Cheng, L. Xu, H. Li and D. Yan, *Mol. Cancer*, 2024, **23**, 241.
30 L. Du, Z. Xing, B. Tao, T. Li, D. Yang, W. Li, Y. Zheng, C. Kuang and Q. Yang, *Signal Transduct. Targeted Ther.*, 2020, **5**, 10.
31 T. A. Triplett, K. C. Garrison, N. Marshall, M. Donkor, J. Blazeck, C. Lamb, A. Qerqez, J. D. Dekker, Y. Tanno, W.-C. Lu, C. S. Karamitros, K. Ford, B. Tan, X. M. Zhang, K. McGovern, S. Coma, Y. Kumada, M. S. Yamany, E. Sentandreu, G. Fromm, S. Tiziani, T. H. Schreiber, M. Manfredi, L. I. R. Ehrlich, E. Stone and G. Georgiou, *Nat. Biotechnol.*, 2018, **36**, 758–764.
32 E. Dolušić, P. Larrieu, L. Moineaux, V. Stroobant, L. Pilotte, D. Colau, L. Pochet, B. Van Den Eynde, B. Masereel, J. Wouters and R. Frédérick, *J. Med. Chem.*, 2011, **54**, 5320–5334.
33 S. Hua, F. Chen, G. Xu and S. Gou, *Eur. J. Med. Chem.*, 2019, **169**, 29–41.
34 F. Chen, G. Xu, W. Tian and S. Gou, *Biochem. Pharmacol.*, 2021, **193**, 114785.
35 D. E. Chapple, P. D. Boyle and J. M. Blacquiere, *ChemCatChem*, 2021, **13**, 3789–3800.
36 Z. Li, X.-M. Liu, F. Tan, J.-Q. Wang, X. Qiao, Y.-K. Feng, J.-Y. Xu and J.-H. Hao, *J. Med. Chem.*, 2025, **68**, 4352–4372.
37 D. Hoffmann, T. Dvorakova, V. Stroobant, C. Bouzin, A. Daumerie, M. Solvay, S. Klaessens, M.-C. Letellier, J.-C. Renauld, N. Van Baren, J. Lelotte, E. Marbaix and B. J. Van Den Eynde, *Cancer Immunol. Res.*, 2020, **8**, 19–31.
38 Y. Ren, R. Wang, S. Weng, H. Xu, Y. Zhang, S. Chen, S. Liu, Y. Ba, Z. Zhou, P. Luo, Q. Cheng, Q. Dang, Z. Liu and X. Han, *Mol. Cancer*, 2023, **22**, 130.
39 Y. Zhang, S. S. Su, S. Zhao, Z. Yang, C.-Q. Zhong, X. Chen, Q. Cai, Z.-H. Yang, D. Huang, R. Wu and J. Han, *Nat. Commun.*, 2017, **8**, 14329.
40 K. Rohde, L. Kleinesudeik, S. Roesler, O. Löwe, J. Heidler, K. Schröder, I. Wittig, S. Dröse and S. Fulda, *Cell Death Differ.*, 2017, **24**, 83–97.
41 H. K. Matthews, C. Bertoli and R. A. M. De Bruin, *Nat. Rev. Mol. Cell Biol.*, 2022, **23**, 74–88.
42 Y. Xie, J. Jiang, Q. Tang, H. Zou, X. Zhao, H. Liu, D. Ma, C. Cai, Y. Zhou, X. Chen, J. Pu and P. Liu, *Adv. Sci.*, 2020, **7**, 1903323.
43 Y. Zhou, I. N. Bastian, M. D. Long, M. Dow and S. Shalapour, *Proc. Natl. Acad. Sci. U. S. A.*, 2021, **118**, e2025840118.
44 Y. Zhang, S. Liu, F. Guo, S. Qin, N. Zhou, Z. Liu, X. Fan and P. R. Chen, *J. Am. Chem. Soc.*, 2024, **146**, 15186–15197.
45 D. Sirnikova, J. Reynisson, A. Brüning-Richardson and C. Kirby, *Neuro Oncol.*, 2023, **25**, iii21.
46 C. Wu, S. A. Spector, G. Theodoropoulos, D. J. M. Nguyen, E. Y. Kim, A. Garcia, N. Savaraj, D. C. Lim, A. Paul, L. G. Feun, M. Bickerdike and M. Wangpaichitr, *Cancer Metab*, 2023, **11**, 7.
47 G. Zhou, G. Qin, Z. Zhang, H. Zhao and L. Xue, *Front. Immunol.*, 2023, **14**, 1283792.
48 F. Exposito, M. Redrado, D. Serrano, L. M. Montuenga, F. Prosper and A. Calvo, *Cell Death Dis.*, 2024, **15**, 787.
49 Z. Zhang, X. Kong, M. A. Ligtenberg, B. Baars, E. E. Voest, S. Klarenbeek, M. Altelaar and D. S. Peeper, *Cell Rep. Med.*, 2022, **3**, 100655.
50 K. Hänggi, L. Vasilikos, A. F. Valls, R. Yerbes, J. Knop, L. M. Spilgies, K. Rieck, T. Misra, J. Bertin, P. J. Gough, T. Schmidt, C. R. De Almodòvar and W. W.-L. Wong, *Cell Death Dis.*, 2017, **8**, e2588.
51 J. Liang, X. Tian, M. Zhou, F. Yan, J. Fan, Y. Qin, B. Chen, X. Huo, Z. Yu, Y. Tian, S. Deng, Y. Peng, Y. Wang, B. Liu and X. Ma, *Biomaterials*, 2024, **309**, 122608.
52 R. L. Van Ineveld, R. Collot, M. B. Román, A. Pagliaro, N. Bessler, H. C. R. Ariese, M. Kleinnijenhuis, M. Kool, M. Alieva, S. M. Chuva De Sousa Lopes, E. J. Wehrens and A. C. Rios, *Nat. Protoc.*, 2022, **17**, 3028–3055.
53 F. Zhou, B. Feng, H. Yu, D. Wang, T. Wang, Y. Ma, S. Wang and Y. Li, *Adv. Mater.*, 2019, **31**, 1805888.
54 S. Kim, H. Park, E. An, H. Eom, W. Zhang, J. Kim, I. Choi, M. Kwak, P. C. W. Lee and J. Jin, *Adv. Funct. Mater.*, 2023, **33**, 2302825.
55 Z. Lu, N. McBrearty, J. Chen, V. S. Tomar, H. Zhang, G. De Rosa, A. Tan, A. M. Weljie, D. P. Beiting, Z. Miao, S. S. George, A. Berger, G. Saggu, J. A. Diehl, C. Koumenis and S. Y. Fuchs, *Cell Metab.*, 2022, **34**, 1342–1358.
56 S. Tian, H. Xu, X. Wu, Y. Ding, L. Liang, H. Yin, X. Zeng, Y. Liu and W. Zhu, *Eur. J. Med. Chem.*, 2025, **289**, 117470.
57 J. Yang, F. Wang, S. Huang, T. Feng, K. Xiong, Y. Chen and H. Chao, *Angew. Chem., Int. Ed.*, 2025, e202505689.